Novel Approaches to the Construction of Miniaturized Analytical Instrumentation

Marc D. Porter	Iowa State University
Ronald P. O'Toole	Iowa State University
Shelley J. Coldiron	Iowa State University
William D. Deninger	Iowa State University
Randall S. Deinhammer	Iowa State University
Stanley G. Burns	Iowa State University
Glenn J. Bastiaans	Iowa State University
Steve D. Braymen	Iowa State University
Howard R. Shanks	Iowa State University

ABSTRACT

This paper focuses on the design, construction, preliminary testing, and potential applications of three forms of miniaturized analytical instrumentation. The first is an optical fiber instrument for monitoring pH and other cations in aqueous solutions. The instrument couples chemically selective indicators that have been immobilized at porous polymeric films with a hardware package that provides the excitation light source, required optical components, and detection and data processing hardware.

The second is a new form of a piezoelectric mass sensor. The sensor was fabricated by the deposition of a thin (5.5 μm) film of piezoelectric aluminum nitride (AlN). The completed deposition process yields a thin film resonator (TFR) that is shaped as a 400 μm square and supports a standing bulk acoustic wave in a longitudinal mode at frequencies of ~1 GHz. Various deposition and vapor sorption studies indicate that the mass sensitivity of the TFRs rival those of the most sensitive mass sensors currently available, though offering such performance in a markedly smaller device.

The third couples a novel form of liquid chromatography with microlithographic miniaturization techniques. The status of the miniaturization effort, the goal of which is to achieve chip-scale separations, is briefly discussed.

INTRODUCTION

Interest in the design, development, and application of chemical sensors has grown explosively in the past several years (1-3). The impetus for this growth derives from the increasing technological need to perform analytical measurements remote from a central laboratory and in a variety of complex settings. Environmental monitoring and process control serve as examples of such needs. There is a general consensus that such sensors be small-sized, durable, have responses specific to a given analyte or classes of analytes, and be fabricated at low cost. The latter attribute enhances deployment in large numbers or as devices with limited operational lifetimes.

More specific attributes are largely application dependent. In a monitoring application, for example, the response of a sensor may need to be reversible. An irreversible response, however, may facilitate usage for dosimetry purposes. Some applications may require large scale deployment, with sensors located at a large number of sampling sites. Detecting and following contaminant plume migration in an aquifer serves as an example. In such a mode, periodic interrogation of the collected data via a telemetric data link would be preferable. In contrast, the operational machinery and piping in an industrial plant may interfere with a telemetric system, dictating the usage of direct hardwire data links.

The development of durable miniaturized analytical instrumentation for chemical sensing is also critical for meeting the many challenges of life-support in the space program. Issues such as small payloads and operation over a wide range of temperature and pressure are requisite for space exploration and colonization. Specific applications, such as space water management, demand the integration of chemically specific sensors with feedback control systems for continuous process monitoring and adjustment of purification systems. Not only must the sensor hardware exhibit both chemical specificity and sensitivity, it must be integrated "on-line" with the processing system to provide the requisite feedback for system adjustment. Thus, meeting the challenges for the development of sensors with specific performance characteristics will require an increasingly interdisciplinary research strategy, drawing from such fields as synthetic organic chemistry, interfacial chemistry, materials science, and computer and electrical engineering.

This paper presents a progress report of the ongoing sensor development efforts at the Analytical Instrumentation Center at Iowa State University. The status of three related projects are presented, each of which are at various developmental stages. The first two sections also addresses issues related to the interfacial chemistry of the sensors, and how to manipulate coatings to achieve the targeted selectivity.

AU: (1) - Porter

The first project involves the construction and performance characterization of a small-sized fiber optic spectrometer for solution-phase analysis (4). As presently configured, the instrument functions in an absorbance mode as a solid-state, dual-beam spectrometer and is equipped with a custom-designed controller, data processor, and telemetric communications hardware.

The second project focuses on the development of a new form of piezoelectric mass sensor (5). Such sensors exhibit a response at low loading levels that is proportional to the mass of a sorbed analyte. The sensor is based on thin film resonator (TFR) technology, consisting of a thin (5.5 μm) oriented aluminum nitride membrane located between two metal electrodes. The sensor, created by coating the TFR surface with a self-assembled monolayer to demonstrate a primitive form of analyte selectivity, exhibits mass sensitivities that rival those of the most sensitive mass sensors currently available, while offering such performance in an extremely small-sized package (400 μm squares).

The third project involves a departure from the general strategies of the first two, focusing on the design, development, and testing of a miniaturized novel (6) form of ion chromatography. The goal of this project is the integration of the components of conventional liquid chromatography to chip-scale sizes. Such a development would provide a separation step prior to detection via various sensor transduction schemes. The status of this project is updated.

DUAL-WAVELENGTH FIBER OPTIC SENSOR INSTRUMENTATION

One of the many challenges of space exploration is the development of compact, durable and reliable instrumentation for incorporation into a life support system. The focus of this project is on the development of fiber optic sensor instrumentation for monitoring the physiological status of astronauts during extended missions. Conventional analytical instrumentation, however, only partially fulfills these needs. For example, common procedures for direct analysis of important electrolytes and minerals (e.g. sodium, potassium, and calcium) employ flames, plasmas or electrical arcs for sample atomization and excitation, facilitating assay of the target analyte by emission or absorbance (7). These instruments are large and require expendable support materials, i.e. fuel and oxidant gases for flames and plasmas. Since the exploration of space and colonization of extraterrestrial bodies places extreme limitations on payload size, the expansiveness of conventional analytical instrumentation dictates development of novel, miniaturized instrumentation.

Figure 1 depicts the major components of the fiber optic sensor, illustrating its attributes. The attributes derive from the combination of three diverse research areas: fiber optic technology, organic thin-film surface chemistry, and electronic hardware design. The union of these three research areas facilitates the conception, design, and application of integrated, sensitive chemical sensors and hardware processing and telemetry systems.

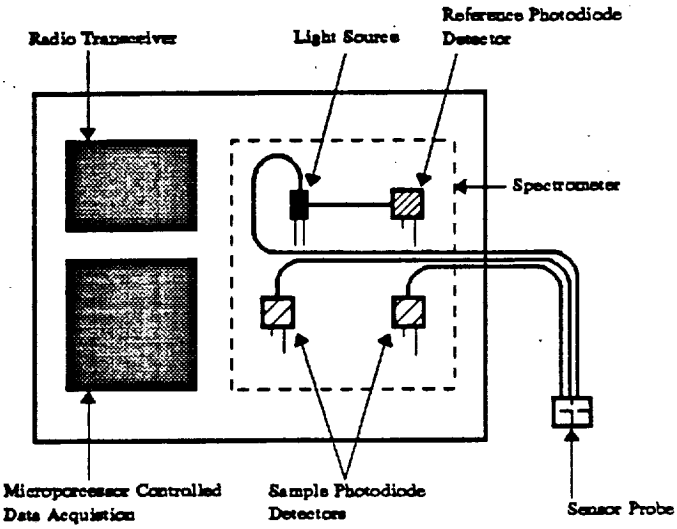

Figure 1. Miniaturized Optical Sensor Instrument.

THIN FILM SENSOR DEVELOPMENT - The development of reversible multicomponent optical electrolyte sensors that can be used for whole blood measurements remains a significant challenge. Current optical pH sensor technology is hampered by the inaccuracies resulting from variations in blood ionic strength (8). Also, since most of the sensor materials are constructed from an impermeable thin film of an organic polymer, response times can be as long as 10 minutes, which limit overall utility.

In earlier work, we first addressed these issues though the development of a highly selective pH sensor (pH range 0-4.5) with a response time of less than 2 sec (9). The sensor was constructed by immobilizing Congo Red at a base-hydrolyzed cellulose acetate film. The rapid response results from the porous structure of the hydrolyzed polymeric support, which reduces barriers to mass transport between the analyte and immobilized indicator. A generalization of the preparative route is shown in Figure 2 and can be readily coupled to other immobilization schemes.

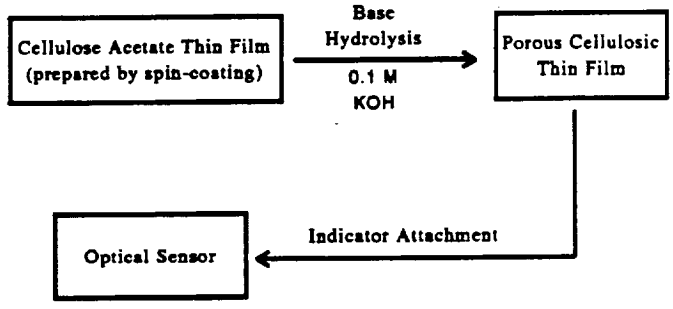

Figure 2. Indicator Immobilization at Porous Cellulosic Films.

Different indicators have been tested for application at physiological pH. Brilliant Yellow, which has an optical transition in solution between pH 6 and 8, was one of the first indicators investigated. However, upon immobilization, the optical transition occurs at higher pH values (i.e. ~2 pH units), an effect frequently observed as a consequence of immobilization (10). Of the many indicators surveyed, fluoresceinamine demonstrated the desired optical transition for detection of physiological pH with immobilization.

Initial indicator attachment techniques with Congo Red utilized non-covalent adsorption of the dye with the cellulosic film (9). However, to increase the long-term stability of the sensor, covalent bonding of the indicator with the film is preferable. Several established linkage techniques were tested such as coupling through cyanuric chloride (11) and cross-linking with glutaraldehyde (12). However, once immobilized, most of the indicators investigated lost their chromophoric transition properties.

The use of polymer beads for coupling and immobilization of indicators is under investigation. Riedel-deHaën produces a polymer carrier for the covalent immobilization of enzymes, Polymer Carrier VA-Epoxy BIOSYNTH®. Chemically, it is a copolymer based on vinyl acetate and divinylethylene-urea whose surface is modified with oxirane groups after hydrolysis of the acetate groups. These epoxide linkages can be utilized to couple various compounds as depicted in Figure 3.

Acid-catalyzed linkage with hydroxyl groups.

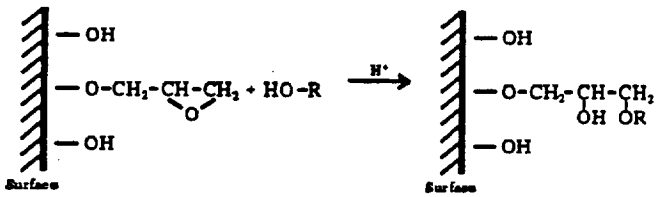

Base-catalyzed linkage with amine groups.

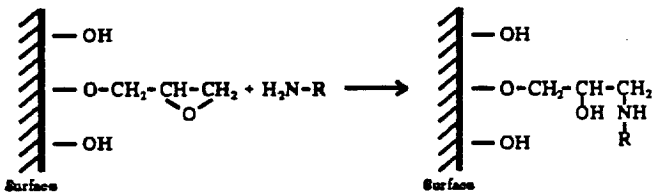

Figure 3. Acid and Base Reactions of Epoxide Linkages.

Fluoresceinamine was coupled to the epoxy beads by weighing 1:1 indicator to bead weight followed by immersion in 1 M Na_2HPO_4. The suspension was stirred for 48 h and excess dye was removed by washing the beads with 0.1 M Na_2HPO_4. The dried product was suspended in a 14% w/w cellulose acetate/cyclohexanone solution. The suspension was sonicated to disperse the beads within the viscous solution. The cellulosic suspension was cast by spin coating onto a glass slide and dried at 70°C for ~12 h. The dried films were then hydrolyzed with 0.1 M KOH for 24 h.

The beads lend strength to the cellulosic films and are easily handled. Without the beads, the films are mechanically weak. The films exhibit both visible and fluorescent spectroscopic transitions with changes in pH from 3 to 9. The indicator behaves as a polyprotic acid with absorption maxima at 440 nm, 460 nm, and 500 nm, which will facilitate the development of an internally calibrated sensor by calculating the ratio of the absorption maxima for each form of the indicator. Such an approach also compensates for calibration difficulties that may arise from preparative variations in the amount of immobilized indicator and the desorption loss of the indicator from the film during use.

INSTRUMENT DEVELOPMENT - Photometer Design - A schematic diagram of the photometer is shown in Figure 4. White light from a miniature lamp is carried to the sensor probe by a single-stranded optical fiber. Another fiber carries a portion of the light from the lamp to a reference detector. Two single-stranded fibers collect and transmit light from the sensor probe to the sample detectors. This design represents a variation from the original prototype which used light emitting diodes as light sources and several other optical components (4). The revised prototype enhances light throughput and utilizes electrical components with greater sensitivity and stability, thereby improving overall instrument sensitivity.

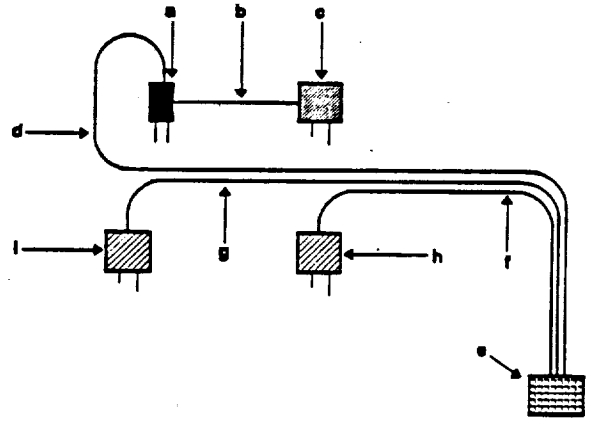

Figure 4. Photometer Schematic. a) White Light Source; b) Single Fiber to Reference Detector; c) Reference Detector; d) Single Fiber to Sensor Probe; e) Sensor Probe; f & g) Fibers to Signal Detectors; h & i) Signal Detectors with Interference Filters.

The light source is a miniature, gas-filled tungsten lamp from Carley Lamps (#T 11/2, 631L). The greybody radiator emits over the visible spectral range. An end lens on the lamp minimizes energy loss from refraction. Additionally, the lamp is positioned within an elliptical reflector (Carley Lamps, #1580) to focus and collimate energy that would be lost through spherical radiation. As described in our earlier work, the collimated beam is focused by a graded refractive

index lens (GRIN) onto the tip of the optical fiber that illuminates the sensor probe (4).

The detector housings (see Figure 5) contain silicon photodiodes (EG&G VACTEC, VTB 9414) with active areas of 1.6 mm^2. The sample detectors measure the light intensity after passing through the sensor probe. The reference detector measures the intensity of the light directly from the lamp. Light from the optical fibers are coupled to interference filters. The selected spectral band is focused upon the detectors with GRIN lenses. The photodiodes are enhanced in the UV to IR spectral range with low dark currents and very high shunt resistances to provide a very low offset in high gain transimpedance connected operational amplifier circuits.

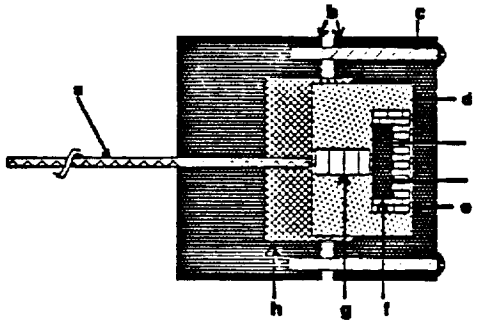

Figure 5. Detector Housing Assembly. a) Single Fiber; b) PVC Assembly Body Housing; c) Nylon Screws; d) Delrin Filter Adapter; e) Delrin Detector Housing; f) Photodiode; g) GRIN Lens; h) Interference Filter.

The photodiodes are connected in a photovoltaic mode to transimpedance operational amplifiers (AD549, Analog Devices). The amplifiers have a common-mode impedance of 10^{15} ohms with an extremely low bias current of 250 fA maximum. The operational amplifier performs well as a sensitive photodiode preamplifier because of its low input current and offset voltage characteristics. Gain is achieved with use of feedback resistance.

The optical fibers have a 400 μm silica core diameter, which is coated by a 80 μm thick fluorine doped silica cladding (UV400/480N, Ceramoptec). The ends of the fibers are polished to a mirror like finish prior to connection with successive grades (32, 15, 3, and 0.3 μm) of abrasive sheets. The all silica construction of the fibers enhances spectral transmission from the UV to IR spectral range over standard communication optical fibers.

Sensor Probe Design - A diagram of the sensor probe is shown in Figure 6. The probe body is constructed from two Delrin discs (1.6 cm diameter and 0.64 cm thick). The top plate serves as a mount for both the input and the collection fibers. The bottom plate houses a GRIN lens. The distal surface of the GRIN lens is coated with a reflective silver film (800 nm thick), which is protected from solution by a coating of epoxy cement. A Nylon plate (0.1 cm thick) is used to mount the thin-film sensor firmly on top of the GRIN lens; a 0.15 cm diameter hole is drilled through the plate to expose a portion of the sensing film to solution and to the incident light beam. Nylon guide pins facilitate optical alignment of the fibers with the GRIN lens and control the separation distance between the Delrin plates. The spacing between the fibers and the thin sensing film (~0.5 cm) provides a clear path for solution to flow over the sensing element. Fully assembled, the probe is 1.7 cm in length and 1.6 cm in diameter.

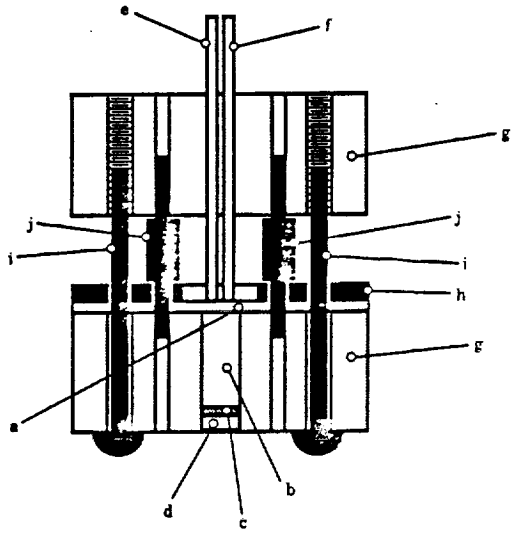

Figure 6. Fiber Optic Sensor Probe. a) Sensing Film; b) GRIN lens; c) Silver Film Mirror; d) Epoxy Cement; e) Input Fiber; f) Collection Fibers; g) Probe Body; h) Retainment Plate; i) Locking Screws; j) Guide Pins.

The GRIN lens steers light from the input fiber of the sensor probe to the collection fibers. To maximize light coupling, the fibers are spaced at an equal distance radially around the lens. The mirrored back surface of the lens serves to reflect the incident radiation. It is important to note that the sampling beam makes two passes through the sensing film prior to transmission back to the photometer.

ADVANTAGES AND ADDITIONAL APPLICATIONS - Advantages - The conceptual basis of these sensors offers several major technological advantages in addition to those described. First, the use of fiber optic sensors facilitates miniaturization of instrumentation. These devices could conceivably be modified and reduced in size for implantation thereby facilitating continuous monitoring of physiological parameters. Miller demonstrated short term biocompatibility of fiber optic sensors for implantation in dogs during a 4 hour catheterized femoral artery study by coating the fibers with a layer containing covalently bonded heparin to prevent thrombosis (13).

Secondly, electrical isolation of these proposed devices provide an added safety feature by prevention of electrical shock. A major concern of invasive devices (e.g. catheters) is inducement of microshock. When the epidermal layer is violated, small currents (on the order of microamps) conducting across heart muscle can lead to fibrillation (14). Fibrillation, unless intervened by defibrillation procedures, can lead to a 'heart attack' and death (14).

Additional Applications - The sensor device described within this paper could be modified for detection of other

analytes. In the sustainable biosphere of a space station or lunar colony, air and water will need to be continuously repurified and recirculated, demanding reliable methods for monitoring removal of toxic wastes and contaminants (15).

As configured, the instrument contains no mechanical components and operates in a fixed-wavelength mode, while maintaining the precision and accuracy of earlier reported fluorescence-based laboratory measurements (16). Based upon construction with low-cost components, small size, mechanical durability, and minimal need for calibration, the instrument would be aptly suited for field deployment in environmental applications. The device could serve as a prototype for development of sensors to detect environmental analytes. Conceivably, modifications would entail: identification and immobilization of proper indicator compounds, replacement of optical filters for different spectral response ranges, and encasement of the hardware package for operation in hostile locations.

Efforts to construct "remote sensing modules" (RSMs) that will use the photometer as the central component are nearing completion. The RSMs, will contain on-board microprocessors for instrument control and FM-radio transceivers for data transmission to a centralized computer system. The microprocessors will control photometer operation and the transceivers will provide wireless data communications.

THIN FILM RESONATORS : A NEW FORM OF PIEZOELECTRIC MASS SENSORS

Piezoelectric mass sensors are solid state devices that respond to changes in temperature, pressure, and most importantly, the physical properties of its interface. Such changes include interfacial mass density, elasticity, viscosity, and sorbed layer thickness. The sensors operate by monitoring the propagation of an acoustic wave through the solid state device. A most common mass sensor is an acoustic bulk wave resonator which is constructed by depositing metal electrodes onto a thin piezoelectric material.

This section briefly summarizes the results of feasibility studies which have established currently achievable mass sensitivities and demonstrated the potential of TFRs as the transducer component in a gas phase chemical sensor. The sensor is based on thin film resonator technology (5, 17-20), consisting of an oriented aluminum nitride membrane situated between two metal electrodes. The sensor has a high mass sensitivity, (S_m, ~550 cm^2/g), is small in size, is easily fabricated, and can potentially be mass-produced at low cost. Using microlithographic techniques, gold-coated TFRs were produced as 400 μm squares with a 5.5 μm membrane thickness (Figure 7). Such small sizes open the possibility of integrating as many as 200 TFRs and associated support electronics onto a single 76 mm diameter silicon wafer. The membrane thickness lead to resonance frequencies of ~1 GHz. As will be demonstrated, these high resonance frequencies translate to mass sensitivities that rival those of the most sensitive mass sensors currently available, while offering such performance in an extremely small-sized package.

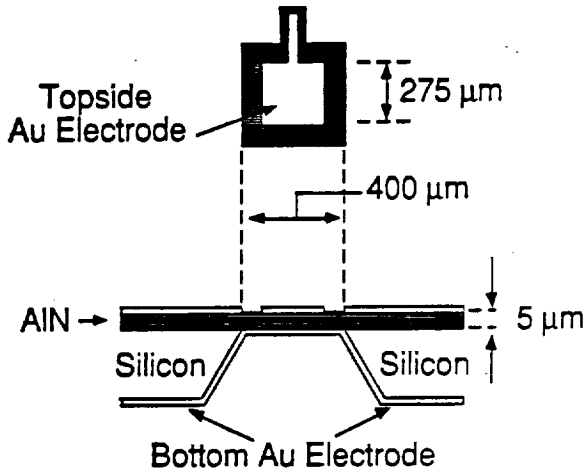

Figure 7. Schematic diagrams of a thin film resonator. The upper portion is a top view where the Au electrode is shown in white and the underlying AlN membrane is shown by the hatch-markings. The lower portion is a side view which illustrates the layered structure of the composite material. See references 5, 17-20 for preparation details.

Sauerbrey first demonstrated that acoustic bulk wave resonators could be used as mass sensors (21). As shown by the classic Sauerbrey equation (Eqn. 1), the relative change in series resonance frequency is linearly related to the mass of a material sorbed on a resonator surface (21, 22), $F°_s$ is the initial series resonance frequency, ΔF_s is the change in series resonance frequency after the deposition of the material, ΔM represents the change in mass per unit surface area arising from analyte sorption, ρ_s is the density of the resonator material, and C_s is the stiffness constant of the membrane. A negative sign on the right hand side of Equation 1 therefore indicates that F_s decreases with increases in sorbed mass. It is important to note that Equation 1 is accurate only for mass depositions less than 2% of the mass of the resonator (22-24) and neglects any effects of differences in the elasticity and/or viscosity of the sorbed material with respect to the resonator material (25-28).

$$\frac{\Delta F_s}{F_s^\circ} = \frac{-2F_s^\circ \Delta M}{[\rho_s C_s]^{1/2}} \qquad (1)$$

The mass sensitivity, S_m, of a bulk acoustic wave resonator is defined, following Wenzel and White (29), as

$$S_m = -\frac{2nF_s^\circ}{\rho_s V} \qquad (2)$$

where n is an integer designating the resonance mode and V is the velocity of the acoustic wave. Since S_m is inversely proportional to resonator thickness, the AlN TFRs are

predicted to have an extremely high mass sensitivity (see Table I).

Table I. Performance Characteristics of Various Piezoelectric Mass Sensors.

Device	Operating Frequency (MHz)	Calculated S_m(cm^2/g)	Experimental S_m(cm^2/g)
QCM[a]	6	-14	-14[d]
SAW[b]	112	-151	-91[e]
	200	-252	-263[f]
	400	-505	-493[f]
FP[c]	2.6	-951	-990[g]
TFR	965	-567	-509[h,i]
	982	-574	-555[j]

a) Quartz Crystal Microbalance. b) Surface Acoustic Wave. c) Flexural Plate. d) Reference 23. e) Reference 39. f) Reference 40. g) Reference 29. h) See reference 5 for a description of measurement protocols. i) PMMA loading experiments (film thickness of 21.7 $\pm$ 0.7 nm). j) Monolayer loading experiments (based on the difference in F_s for films formed by the spontaneous adsorption of $CH_3(CH_2)_3SH$ and $CH_3(CH_2)_{17}SH$).

MASS SENSITIVITY (S_m) TESTS - The sensitivity of the TFRs to mass loading was determined by two different experiments, the results of which are summarized in Table I. The first experiment monitored the effect of the deposition of a 21.7 $\pm$ 0.7 nm film of PMMA on the resonator properties. Measurements were taken on several TFRs with typical absolute and relative frequency changes after coating of 35 kHz and 39 ppm, respectively. Based on the coating thickness and the density of bulk PMMA (1.2 g/cm^3) (30), ΔM was calculated.

In the second experiment, the TFR response was first measured after adsorption of a monolayer formed from butanethiol ($CH_3(CH_2)_3SH$). The TFRs were next cleaned and coated with a monolayer from octadecanethiol ($CH_3(CH_2)_{17}SH$). The TFR responses were again measured. Since both monolayers form structures with comparable surface coverages (9.1 $\pm$ 0.5 x 10^{-10} moles/cm^2 (31, 32)), the difference in mass loading between the two monolayers was calculated from their chain length differences. Such tests using uncoated TFRs were hindered because of contaminant adsorption at the "bare" gold surface.

From the results of the two different mass loading experiments, experimental values of S_m were calculated. Equation 2 was used to compute a S_m based on F_s and literature values of ρ_s and V (33). Table I summarizes the results and provides comparison data for other forms of piezoelectric mass sensors. As is evident, the average experimentally determined values of S_m (-509 and -555 cm^2/g) are comparable to those predicted by theory (-567 and -574 cm^2/g), consistent with the performance expected for a well-behaved mass sensor. More importantly, these results show that the TFRs exhibit a much greater intrinsic sensitivity to mass loading than the QCMs. Only the flexural plate and the high frequency (i.e., 400 MHz) SAW devices, which are both markedly larger in size and have much more complex electrode patterns, have comparable sensitivities.

DEMONSTRATION OF PERFORMANCE OF TFRs AS A GAS PHASE SENSOR - As is the case for many types of chemical sensors, the performance of piezoelectric mass sensors is as much or more a function of the surface coating as it is of the mass response characteristics. The properties of the coating determine the rate of the response, reversibility, and selectivity. The coatings also play a major role in defining the relationship between analyte concentration and analytical response. Therefore, the choice of the coating is one of the most critical aspects of sensor design. To demonstrate the feasibility of using TFRs as sensors, two relatively simple sets of experiments were designed. The first used monolayers formed from a fluorinated thiol ($CF_3(CF_2)_7(CH_2)_2SH$) and a carboxylic acid-terminated thiol ($HO_2C(CH_2)_{15}SH$). The second, described elsewhere (5), employed coatings of PMMA. Both sets of experiments used methanol as a gas phase analyte for testing performance.

The goal of the monolayer-coating experiments was to exploit the differences in the interfacial properties of the two terminal groups, thereby gaining a degree of selectivity in the adsorption of methanol vapor. Fluorinated monolayers have critical surface tensions of 5-10 mN/m (34), values indicative of a very low free surface energy. These monolayers are not wetted by methanol, and therefore should display limited affinity for the sorption of methanol vapor. Conversely, the carboxylic acid-terminated monolayer presents a much more reactive functional group at the air-monolayer interface (35). These films are wetted by methanol, a result of both the polarity and hydrogen-bonding capability of the end group. Based on wettabilities, the TFRs coated with the carboxylic acid-terminated monolayer should interact strongly with methanol, whereas those coated with the fluorinated monolayer should exhibit a lower affinity.

To test the methanol-exposure responses, TFRs were sequentially cleaned, tested with the fluorinated monolayer, cleaned, and tested with the carboxylic acid monolayer. In each run, the TFRs were equilibrated in a dry, flowing Ar atmosphere and then exposed to three different concentrations of methanol separated by flushes with Ar. Responses are shown in Figure 8A for the fluorinated monolayer and Figure 8B for the carboxylic acid-terminated monolayer. Rapid changes in $\Delta F_s/F^\circ_s$ are observed for both monolayers upon the introduction and removal of methanol from the test chamber. The responses return to their initial values upon removal of methanol, indicating that the sorption of methanol is reversible at both monolayers. The magnitude of the response of the carboxylic acid-terminated monolayer is, however, much larger than that of the fluorinated monolayer. The response differences are consistent with the behavior

predicted by wettability data, pointing to the potential use of monolayers designed for molecular recognition purposes (36, 37) as selective or class specific coatings for sensor applications. More importantly, these findings confirm the feasibility of using TFRs as mass sensors.

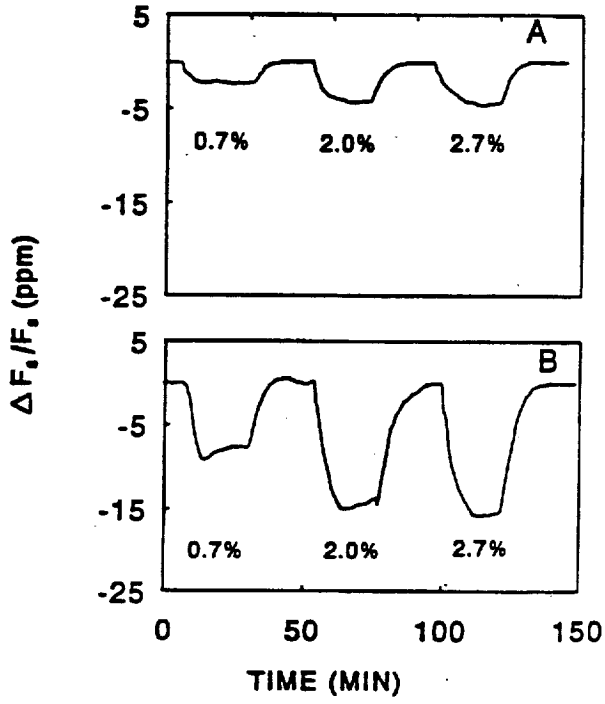

Figure 8. Baseline-corrected responses of TFRs with hydrophobic and hydrophilic surfaces to methanol. A) TFR coated with fluorinated thiolate. B) TFR coated with carboxylic acid-terminated thiolate. Responses are expressed as relative changes (i.e. $\Delta F/F°_s$) using units of parts per million (ppm). Note that the response times reflect a mixture of processes, including the evaporation of methanol and the removal of methanol from the test chamber. Measurement instabilities, such as those that may arise from small temperature changes, have been accounted for using a six-point baseline linearization.

It is also interesting to note that the TFR response for both monolayers is nonlinear with methanol concentration. This behavior indicates that the surface coverage of sorbed species approaches saturation at the larger methanol concentrations. Interestingly, one can predict the saturation coverage of methanol for the carboxylic acid-terminated monolayer by assuming that each acidic functionality can bind with one methanol molecule. Since the surface coverage of these monolayers is $9.1 \pm 0.5 \times 10^{-10}$ moles/cm^2 (31, 32), the saturated coverage of methanol would translate to mass increase of 29 ng/cm^2. In Figure 8B, the maximum response of the acid-coated TFR was -12.7 ppm. This frequency change corresponds to a mass increase of 23 ng/cm^2, using the average experimental S_m value of -555 cm^2/g from Table I. Thus, it appears that the acid-terminated layer approaches a 1:1 binding stochiometry with methanol: This finding suggests that, in addition to sensor application, the TFRs may potentially find uses in fundamental studies of wetting, condensation, and a host of other important interfacial processes.

CHIP-SCALE ION CHROMATOGRAPHY

The long term goal of this project is the development of a microminiature liquid chromatograph on a silicon wafer. Such instrumentation would provide an attractive approach for environmental assessment and monitoring programs as well as the space program. Though far from completion, we envision an instrument that represents an integration of the components (e.g., injector, pump, column with chemically specific stationary phase, and detector) of conventional liquid chromatographs, though at an extreme of miniaturization. The focus of this project is several-fold. The key areas include the development of techniques for trenching small diameter (10-50 μm) columns at standard sized (76 mm) silicon wafers, for flowing solution through the columns, and for chemically modifying the walls of the columns. Each of the objectives has been accomplished to varying degrees. Trenches of the specified size have been fabricated by a combination of photolithographic and chemical etching methods. Trenches with, for example, a nominal diameter of 15 μm have been prepared, with the topography characterized by both scanning electron and atomic force microscopies. A cross-sectional view of an etched half-cylinder column is shown in Figure 9. As presented, a silicon wafer has been direct bonded to the trenched bottom-wafer to complete column fabrication. Attempts to seal two such trenches together to form a cylindrical column have met with difficulties with respect to alignment registry. Infrared imaging may overcome this difficulty.

To control the flow of solution through these columns, we have constructed a pneumatic pumping system. The pumping system provides a low flow rate (a few nL/min). The flow rate can be regulated by varying the pressure of an inert gas at the liquid in contact with the entrance channel of the column. A microelectrode, prepared by the evaporation of a small gold disk at the exit channel of the column, served as the detector for this characterization. Unexpectedly, these columns were easily plugged by small-sized particulate matter that is difficult to remove even after filtering the solutions by passage though a with a 10 μm membrane filter. We are currently devising methods to overcome this complication.

Several routes for the chemical modification of the walls of the columns have been devised, with the goal to manipulate separations in a fashion analogous to that used in conventional chromatography as well as with our recently developed electrochemically-based approach (6). The most promising approach utilizes established silane chemistry (38). In this scheme, silicon with a native oxide is exposed to an anhydrous solution containing an end-group (X) functionalized trichlorosilane ($X(CH_2)_nSiCl_3$). Through a reaction with the hydroxyl groups of the native oxide, a two-dimensional network of a cross-linked monolayer is formed.

Verification of the successful functionalization of the silicon surface with monolayers of various end-groups was obtained using infrared reflection spectroscopy and wettability measurements. These characterizations were performed on large-sized replicates of the surface of the trenched materials. We hope to report "proof of concept" in the near future.

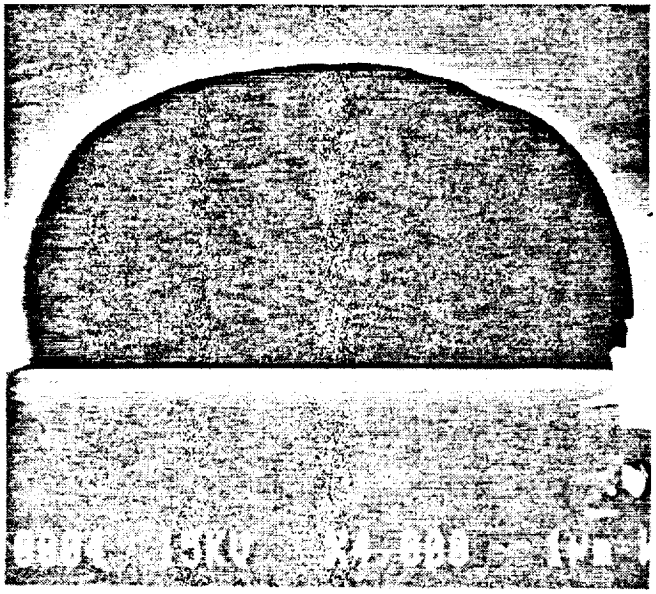

Figure 9. Scanning electron micrograph of etched trenches in silicon.

ACKNOWLEDGMENTS

M.D.P. expresses appreciation for the support of a Dow Corning Assistant Professorship, S.J.C. for a NASA/Iowa Space Grant Fellowship through the College Consortium under the NASA Space Grant Program, and R.P.O. for a Harpole Graduate Fellowship through the Department of Electrical Engineering at ISU. This work was supported in part by the Center for Advanced Technology Development at Iowa State University under USDOC Grant ITA 87-02, by the Office of Basic Energy Research-Chemical Sciences Division of USDOE, and by the Advanced Life Support Division of the NASA-Ames Research Center (Contract No. NAG2-722. Ames Laboratory is operated for the U. S. Department of Energy by Iowa State University under Contract No. W-7405-Eng-82.

REFERENCES

1. Edmonds, T. E., Ed., *Chemical Sensors*; Blackie: Glasgow, 1988.

2. Turner, A. P. F., Karube, I., Wilson, G. S., Eds., *Biosensors Fundamentals and Applications*; Oxford University Press, Oxford, 1987.

3. Janta, J. *Anal. Chem.* **1990**, *62*, 33R-44R.

4. Jones, T. P., Coldiron, S. J., Deninger, W. J. and Porter, M. D. *Appl. Spectrosc.* **1991**, *45*, 1271-77.

5. O'Toole, R. P., Burns, S. G., Bastiaans, G. J., Porter, M. D. *Anal. Chem.* **1992**, *63*, 1289-95.

6. Deinhammer, R. S., Shimazu, K., Porter, M. D. *Anal. Chem.* **1991**, *63*, 1889-94.

7. Ingle, J. D. and Crouch, S. R., *Spectrochemical Analysis*, Prentice Hall, Englewood Cliffs, New Jersey, 1988.

8. Collison, M. E. and Meyerhoff, M. E. *Anal. Chem.* **1990**, *62*, 425A-37A.

9. Jones, T. P. and Porter, M. D. *Anal. Chem.* **1988**, *60*, 404-406.

10. Stole, S. M., Jones, T. P., Lai-Kwan, C., and Porter, M. D., in *Chemical Sensors and Microinstrumentation*, Murray, R. W., Dessy, R. E., Heineman, W. R., Janta, J., and Seith, W. R., Eds: American Chemical Society Symposium Series No. 403, Washington, D.C. , 1989

11. Saari, L.A. *Anal. Chem.* **1982**, *54*, 823-4.

12. Zhujun, Z., Zhang, Y., Wangbai, M., Russell, R., Shaksher, Z. M., Grant, C. L., and Seitz, W. R. *Anal. Chem.* **1989**, *61*, 202-5.

13. Miller, W. W. *Clin. Chem.* **1987**, *54*, 823-4.

14. Webster, J. G., *Medical Instrumentation*, Houghton Mifflin Company, Boston, 1978.

15. Johnston, R. S. and Dietlein, L. F., Eds., *Biomedical Results from Skylab*, NASA SP-377, 1977.

16. Luo, S., and Walt, D. R. *Anal. Chem.* **1989**, *61*, 174-178.

17. Burns, S. G., Weber, R. J., Brayman, S. D., in *Proceedings of the 45th IEEE Symposium in Frequency Control*, **1991**, 207-11.

18. Wang, J. S., Lakin, K. M. *Appl. Phys. Lett.* **1982**, *40*, 308-10.

19. Burns, S. G., Ketcham, R. S. *IEEE Trans. Microwave Theory Tech.* **1984**, *32*, 1668-71.

20. Wang, J. S., Lakin, K. M. *IEEE Proceedings of the 1981 Ultrasonics Symposium*, 502-5.

21. Sauerbrey, G. *Z. Physik* **1959**, *155*, 206.

22. Benes, E. J. *Appl. Phys.* **1984**, *56*, 608-26.

23. Lu, C-S, Lewis, O. J. *J. Appl. Phys.* **1972**, *43*, 4384-4390.

24. Crane, R. A., Fisher, G. *J. Phys. D: Appl. Phys.* **1979**, *12*, 2019-26.

25. Kanazawa, K. K., Gordon, J. G. *Anal. Chim. Acta* **1985**, *175*, 99-105.

26. Bruckenstein, S., Shay, M. *Electrochimica Acta* **1985**, *10*, 1295-1300.

27. Beck., R., Pittermann, U., Weil, K. G. *Ber. Bunsenges. Phys. Chem.* **1988**, *92*, 1363-68.

28. Schumacher, R. *Angew Chemie*, Internat. Ed., **1990**, *29*, 329-438.

29. Wenzel, S. W., White, R. M. *Appl. Phys. Lett.* **1989**, *54*, 1976-78.

30. Bradrup, J, Immergut, E. H., Eds.; *Polymer Handbook*; Wiley, New York, 1975, 2nd Ed.

31. Widrig, C. A., Chung, C., Porter, M. D. *J. Electroanal. Chem.* **1991**, *113*, 2805-10.

32. Walczak, M. M., Popenoe, D. D., Deinhammer, R. S., Lamp, B. D., Chung, C., Porter, M. D. *Langmuir* **1991**, *7*, 2687-93.

33. Krishnaswamy, S. V., Rosenbaum, J., Horwitz, S., Vale, C., Moore, R. A. *IEEE Proceed. 1990 Ultrasonics Symposium*, New York, **1990**, 529-36.

34. Shafrin, E. G., Zisman, W. A. *J. Phys. Chem.* **1960**, *64*, 519-28.

35. Whitesides, G. M., Laibinis, P. E. *Langmuir* **1990**, *6*, 87-96.

36. Rubenstein, I., Steinberg, S., Yitzhak, T., Shanzar, A., Savig, J. *Nature* **1988**, *332*, 426-29.

37. Arduengo, A. J., Moran, J. R., Rodriguez-Parada, J., Ward, M. D. *J. Am. Chem. Soc.* **1990**, *112*, 6153-54.

38. Netzer, L., Sagiv, J. *J. Am. Chem. Soc.* **1983**, *105*, 674-81.

39. Wohltjen, H., Snow, A. W., Barger, W. R., Ballantine, D. S. *IEEE Trans. Ultrasonics. Ferroelectric Freq. Control* **1987**, *343*, 172-78.

40. Grate, J. W., Klusty, M. *Anal. Chem.* **1991**, *63*, 1719-1727.